ISSN 1064-2269, Journal of Communications Technology and Electronics, 2019, Vol. 64, No. 1, pp. 1–12. © Pleiades Publishing, Inc., 2019.
Russian Text © Yu.I. Bova, A.S. Kryukovsky, D.S. Lukin, 2019, published in Radiotekhnika i Elektronika, 2019, Vol. 64, No. 1, pp. 3–14.

ELECTRODYNAMICS AND WAVE PROPAGATION

Propagation of Frequency-Modulated Electromagnetic Radiation in the Earth's Ionosphere with Allowance for Absorption and the External Magnetic Field

Yu. I. Bova[a], A. S. Kryukovsky[a, *], and D. S. Lukin[a]

[a] *Russian New University, Moscow, 105005 Russia*

**e-mail: kryukovsky56@yandex.ru*

Received January 09, 2018; Revised January 09, 2018; Accepted February 28, 2018

Abstract—Propagation of frequency-modulated signals in an anisotropic medium (Earth's ionosphere) is numerically simulated with allowance for the effect of the electron collision frequency on deflecting absorption. Projections of ray paths onto different coordinate planes are considered. The influence of the divergence of the ray paths and absorption of radio waves on the attenuation of the radio signal for ordinary and extraordinary waves is studied. The calculations were performed for the daytime and nighttime models of the electron density and collision frequency of the high-latitude ionosphere.

DOI: 10.1134/S1064226919010030

INTRODUCTION

Decameter electromagnetic waves are widely used for long-range radio communications, radio navigation, radar, beyond-the-horizon surveillance, and investigation of the ionosphere: the Earth's upper atmosphere. Therefore, the propagation of such waves attracts much attention of researchers. However, despite a significant amount of publications on this subject (see, e.g., [1–7]), the propagation of frequency-modulated (FM) signals in the ionospheric plasma with allowance for the Earth's magnetic field has been studied insufficiently.

Earlier [8–13], we considered the features of the ray propagation of frequency-modulated radiation in the ionospheric plasma. In the present paper, which is devoted to modeling the propagation of a linearly frequency-modulated (chirp) signal in an ionospheric anisotropic plasma, special attention is paid to the attenuation of the radio signal due to deflecting absorption and divergence on the example of models of electron density and electron collision frequency for the high-latitude nighttime and daytime ionosphere.

1. MATHEMATICAL FORMULATION OF THE PROBLEM

It is known that the effective permittivity of a medium of an inhomogeneous anisotropic ionosphere is described by the Appleton formula [14]:

$$\varepsilon = 1 - v\left(1 - iZ - \frac{u\sin^2\alpha}{2(1 - v - iZ)} \pm \sqrt{\frac{u^2\sin^4\alpha}{4(1 - v - iZ)^2} + u\cos^2\alpha}\right)^{-1}, \quad (1)$$

where the plus sign corresponds to an ordinary wave and the minus sign corresponds to an extraordinary wave and the parameters v and u are the ratios of the squared plasma frequency and the squared gyrofrequency to the squared working frequency, respectively; i.e.,

$$v = \left(\frac{\omega_{\text{pl}}}{\omega}\right)^2 = \frac{4\pi e^2 N}{m_e\omega^2}, \quad u = \left(\frac{\omega_H}{\omega}\right)^2 = \frac{e^2 H_0^2}{m_e^2 c^2 \omega^2}, \quad (2)$$

where $c = 2.997925 \times 10^8$ m/s is the speed of light, $m_e = 9.108 \times 10^{-28}$ g is the electron mass, $e = 4.8029 \times 10^{-10}$ CGSE is the electron charge, and the function N is the electron density at a fixed point of space. The parameter Z is the ratio of the electron collision frequency to the working circular frequency:

$$Z = \frac{\nu_e}{\omega}. \quad (3)$$

The quantity α is the angle between the Earth's magnetic field $\vec{H}_0 = (H_{0x}, H_{0y}, H_{0z})$ and the wave vector $\vec{k}$. To apply formula (1), we only need to know $\cos^2\alpha$. The squared cosine of the angle α is determined by the expression

$$\cos^2\alpha = \frac{(H_{0x}k_x + H_{0y}k_y + H_{0z}k_z)^2}{H_0^2\left|\vec{k}\right|^2}. \quad (4)$$

In the calculations below, the amplitude of the magnetic field will be considered constant. The orientation of the magnetic field in the local coordinate system is given by the angles γ and φ:

$$H_{0x} = H_0\cos\gamma\cos\varphi, \quad H_{0y} = H_0\cos\gamma\sin\varphi, \quad H_{0z} = H_0\sin\gamma. \quad (5)$$

If the electron collision frequency can be neglected, i.e., $Z = 0$, the formula for the effective permittivity (see, e.g., [4, 7, 14, 15]) has the form

$$\varepsilon_{\pm} = 1 - \frac{2v(1-v)}{2(1-v) - u\sin^2\alpha \pm \sqrt{u^2\sin^4\alpha + 4u(1-v)^2\cos^2\alpha}}. \quad (6)$$

The approach used in this work is based on ray methods, which are fundamental in describing the processes of propagation of decameter radio waves in various media (see, e.g., [4, 15]). The main ray method for finding ray paths in an anisotropic inhomogeneous medium is the bicharacteristic method, based on the system of differential equations (see [4, 13, 15])

$$\frac{d\vec{r}}{d\tau} = \frac{\partial\Gamma}{\partial\vec{k}}, \quad \frac{d\vec{k}}{d\tau} = -\frac{\partial\Gamma}{\partial\vec{r}}, \quad \frac{dt}{d\tau} = -\frac{\partial\Gamma}{\partial\omega}, \quad \frac{d\omega}{d\tau} = \frac{\partial\Gamma}{\partial t}, \quad (7)$$

with the Hamiltonian

$$\Gamma = k_x^2 + k_y^2 + k_z^2 - \frac{\omega^2}{c^2}\varepsilon_r(\vec{r},\vec{k},\omega), \quad (8)$$

where $\vec{r} = (x, y, z)$ are the coordinates of the observation point, t is the group time, ω is the circular frequency of the radiation, $\vec{k} = (k_x, k_y, k_z)$ is the wave vector, τ is the parameter of the ray path, and $\varepsilon_r(\vec{r},\vec{k},\omega)$ is the real part of the effective permittivity of the medium of propagation.

To apply system (7) and (8), it is necessary to separate the real part of permittivity (1), i.e., represent the permittivity as the sum of the real and imaginary parts:

$$\varepsilon = \varepsilon_r + i\varepsilon_i. \quad (9)$$

Analyzing expression (1), we find

$$\varepsilon_r = 1 - \frac{v(z_\varepsilon + r_\varepsilon\cos\varphi_\varepsilon)}{(z_\varepsilon + r_\varepsilon\cos\varphi_\varepsilon)^2 + (u_\varepsilon + r_\varepsilon\sin\varphi_\varepsilon)^2}, \quad (10)$$

$$\varepsilon_i = \frac{v(u_\varepsilon + r_\varepsilon\sin\varphi_\varepsilon)}{(z_\varepsilon + r_\varepsilon\cos\varphi_\varepsilon)^2 + (u_\varepsilon + r_\varepsilon\sin\varphi_\varepsilon)^2}. \quad (11)$$

In formulas (10) and (11), we use the notation

$$z_\varepsilon = 1 - \frac{(1-v)u\sin^2\alpha}{2((1-v)^2 + Z^2)},$$
$$u_\varepsilon = -Z - \frac{Zu\sin^2\alpha}{2((1-v)^2 + Z^2)}, \quad (12)$$

$$r_\varepsilon = \pm\left(x_\varepsilon^2 + y_\varepsilon^2\right)^{1/4}, \quad \varphi_\varepsilon = \frac{1}{2}\arctan\left(\frac{x_\varepsilon}{y_\varepsilon}\right), \quad (13)$$

$$x_\varepsilon = \frac{(1-v)Zu^2\sin^4\alpha}{2((1-v)^2 + Z^2)^2},$$
$$y_\varepsilon = u\cos^2\alpha + \frac{((1-v)^2 - Z^2)u^2\sin^4\alpha}{4((1-v)^2 + Z^2)^2}. \quad (14)$$

If the external magnetic field is absent ($H_0 = 0$), formula (1) for the permittivity has the form [14]

$$\varepsilon = 1 - \frac{v}{1+Z^2} - i\frac{vZ}{1+Z^2}. \quad (15)$$

Assume that the initial wave vector $\vec{k}(0)$ depends parametrically on the ray departure angle α_0 ($\beta_0 = 0$):

$$k_x(0) = \frac{\omega}{c}\sqrt{\varepsilon_0}\cos\alpha_0\cos\beta_0,$$
$$k_y(0) = \frac{\omega}{c}\sqrt{\varepsilon_0}\cos\alpha_0\sin\beta_0, \quad (16)$$
$$k_z(0) = \frac{\omega}{c}\sqrt{\varepsilon_0}\sin\alpha_0,$$

and the radiation source is a point outside of the magnetoactive plasma with the coordinates

$$\vec{r}\big|_{\tau=0} = (0,0,0). \quad (17)$$

The propagation of an electromagnetic wave initially takes place in the (x, z) plane. Denote the effective permittivity of the medium in the radiation source by ε_0. Assume that the signal is linearly frequency-modulated (chirp); i.e., the formula for the instantaneous carrier frequency has the form [8, 10]

$$\omega(0) = \omega_0(1 + \delta\eta), \quad t(0) = \eta,$$
$$f(t) = f_0(1 + \delta t), \quad \delta = \frac{2f_d}{f_0T_p}, \quad (18)$$

where η is the ray departure time, $f_0 = \omega_0/(2\pi)$ is the initial operating frequency (Hz), f_d is the frequency deviation (Hz), and T_p is the pulse duration (s). In this work, we used the following values of the parameters: $f_0 = 2.5$ MHz, $f_d = 3.75$ MHz, $T_p = 3$ s, and $\delta = 1$ s^{-1}. With such parameters, the maximum radiation frequency is 10 MHz.

Let us consider two models of high-latitude ionospheric plasma: nighttime and daytime. The electron density profile of the nighttime ionosphere (Fig. 1a) has the traditional form: the E layer is poorly visible and the maximum of the F layer is much lower than in the daytime ionosphere. On the contrary, the profile of the daytime ionosphere (Fig. 1b) is atypical, since, at the maximum of the E layer, the electron density is higher than in the F layer.

Figure 2 shows the dependence of the electron collision frequency on the altitude for the nighttime and daytime ionosphere. At low altitudes, these graphs almost coincide. Significant difference begins at alti-

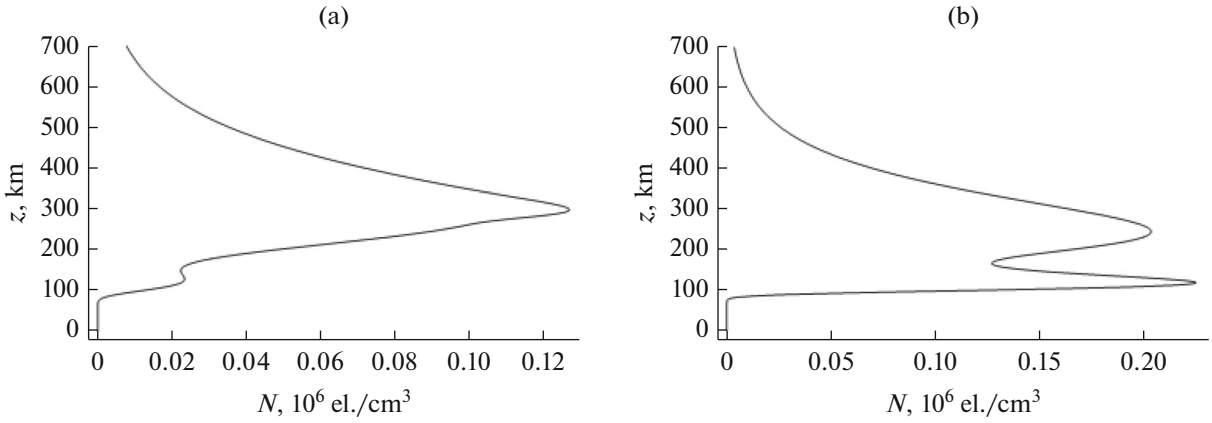

Fig. 1. Electron density vs. altitude for (a) nighttime and (b) daytime models of high-latitude ionospheric plasma.

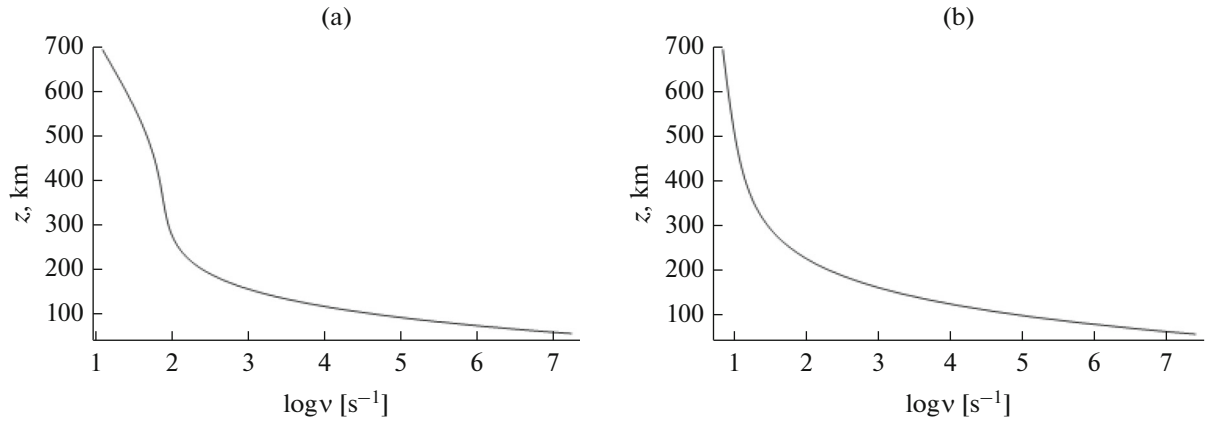

Fig. 2. Electron collision frequency vs. altitude: (a) nighttime and (b) daytime ionosphere.

tudes above 110 km, where the role of the electron collision frequency in absorption (and even more in the deviation of the trajectory) is small.

The profiles presented in Figs. 1 and 2 are consistent with the data given in [16] (80° N, 30° E, March). The calculations were carried out with the following parameters: $H_0 = 0.551$ Oe, $\varphi = \pi/4$, $\zeta = 0$, and $\gamma = -83°$.

2. NUMERICAL SIMULATION. NIGHTTIME IONOSPHERE

In this section, in Figs. 3–9, the results of numerical simulation in the case of the nighttime ionosphere for ordinary and extraordinary waves are presented. The background in all the figures means the electron density in the ionosphere.

Figure 3 shows the radiation structure of a chirp signal in the (*x, z*) plane when the radiation source is situated on the ground. The ray departure angle is 45°. In the region about the altitude of 115 km, the *E* layer is visible. At an altitude of about 290 km, the layer *F*2 is clearly visible. At first, all rays go along a common trajectory. Then, in the ionosphere (dispersing medium) they diverge. Low-frequency rays are reflected from the *E* and *F*2 layers and return to the Earth, and high-frequency rays penetrate through the layer. With increasing frequency, the trajectories become straight.

The ray structures of ordinary (see Fig. 3a) and extraordinary waves (see Fig. 3b) differ insignificantly, but, for an extraordinary wave, the penetration through the ionosphere occurs at higher frequencies than for an ordinary wave.

Figure 4 shows the ray structure of a chirp signal in the (*y, z*) plane. The rays passing through the ionospheric layer *F*2, above 400 km, rotate in parallel to the *z*-axis and go upward (high frequencies).The reflected rays (low frequencies) return to the Earth along close trajectories, since there are no horizontal gradients (within the model). It should be noted that the ray structure of an extraordinary wave (see Fig. 4b) in this plane looks more compact than the structure of an

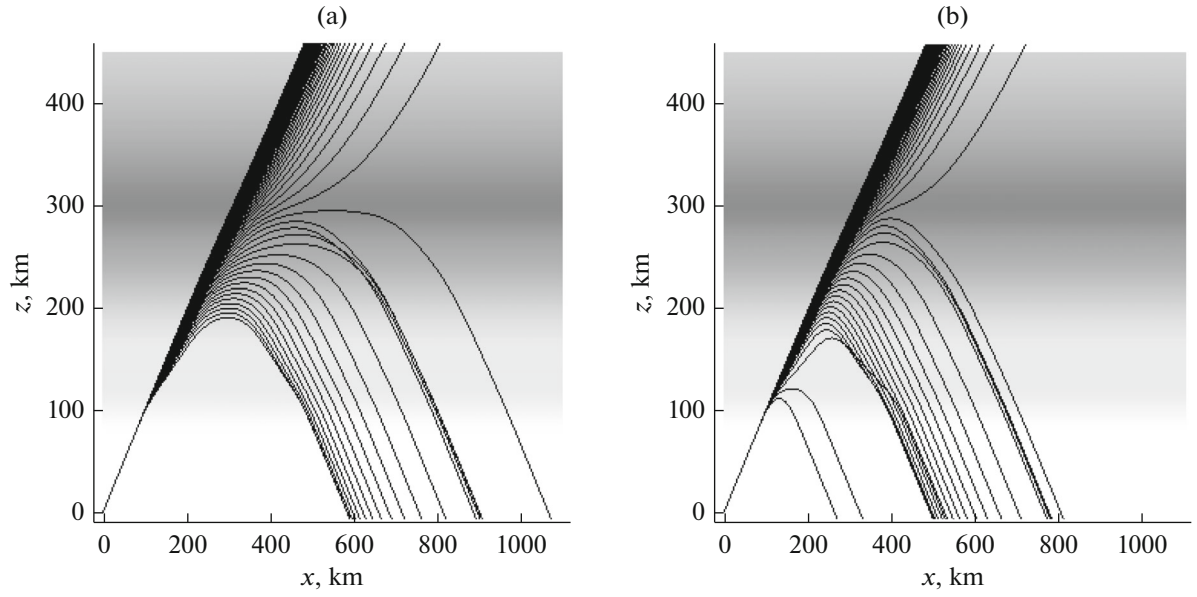

Fig. 3. Ray structure of a chirp signal in the plane (*x, z*); (a) ordinary wave and (b) extraordinary wave.

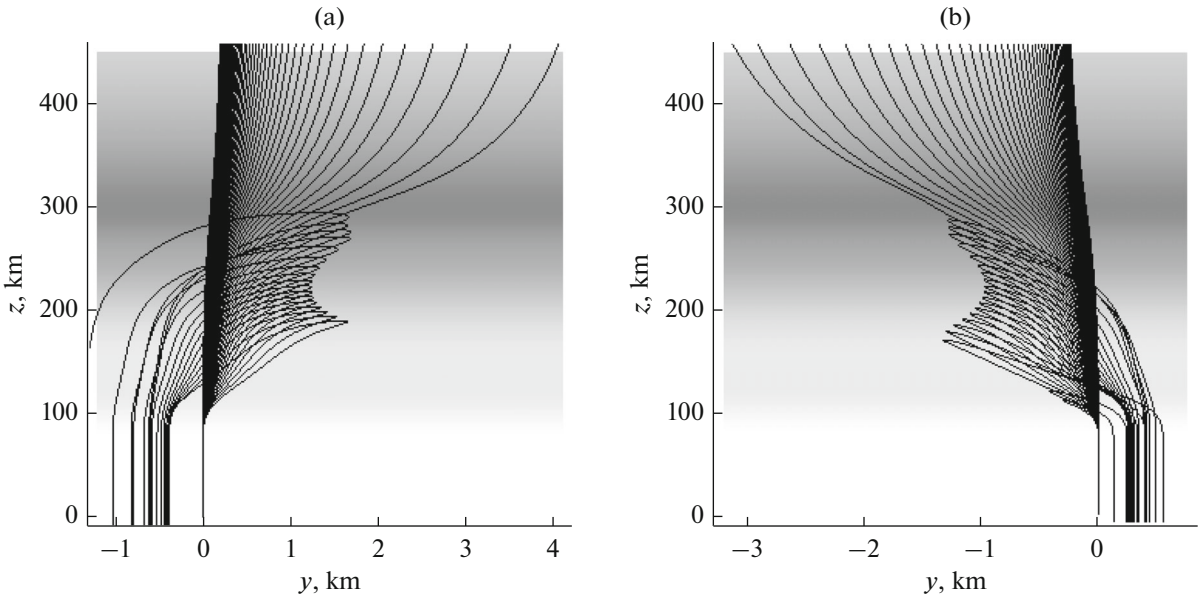

Fig. 4. Ray structure of a chirp signal in the plane (*y, z*); (a) ordinary wave and (b) extraordinary wave.

ordinary wave (see Fig. 4a) and is a sort of its mirror reflection about the vertical axis.

Figure 5 shows the radiation structure of a chirp signal in the (*x, y*) plane. This is a top view of the ray structure. The structure of an extraordinary wave (see Fig. 5b) in this plane is similar to the mirror reflection from the horizontal axis of the structure of an ordinary wave (see Fig. 5a). In the case of an extraordinary wave, the propagation of the signal along the *y*-axis is substantially "more compact". In this projection, we clearly see a caustic structure and its singularity: an A_3 catastrophe. The wave field structure in the vicinity of the caustic tip (A_3 catastrophe) was studied in detail in [17–20].

Let us now consider the absorption along the trajectories. The absorption associated with the electron collision frequency is calculated by the formula

$$\frac{d\Psi}{d\tau} = -2\varepsilon_i \frac{\omega^2}{c^2}. \qquad (19)$$

It should be noted that, at small ratios of the effective electron collision frequency to the working circular

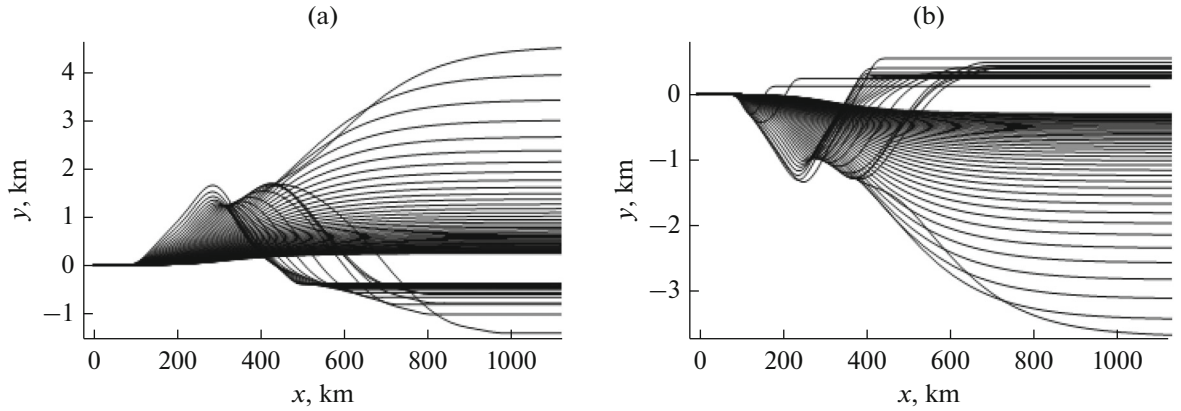

Fig. 5. Ray structure of a chirp signal in the plane (x, y); (a) ordinary wave and (b) extraordinary wave.

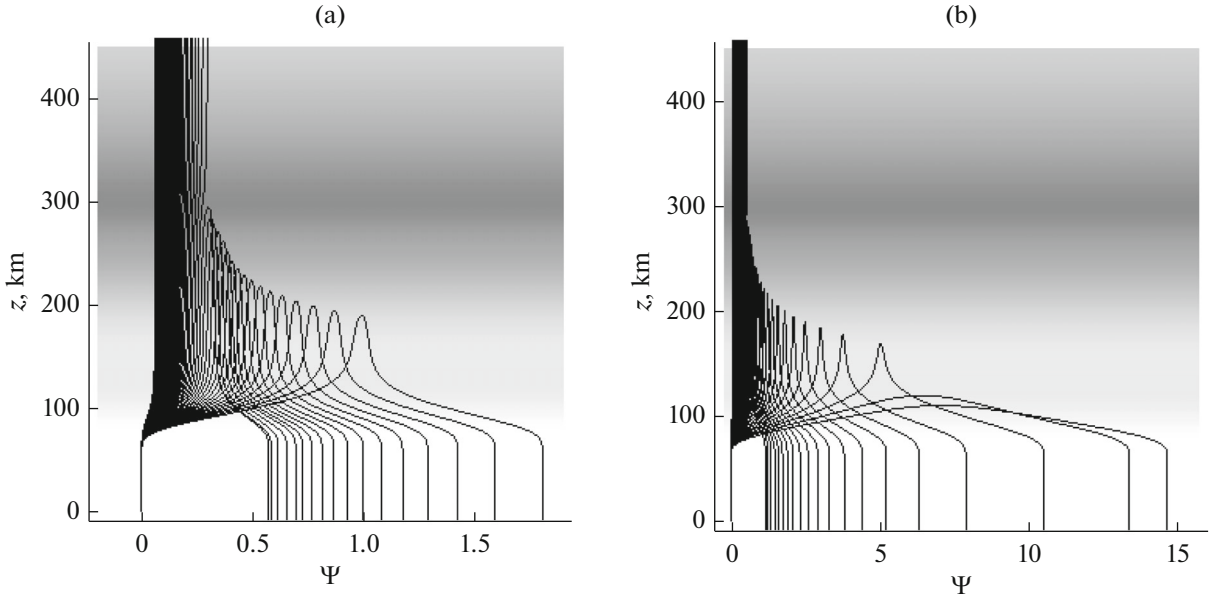

Fig. 6. Absorption Ψ (in Nepers) along trajectories vs. altitude: (a) ordinary wave and (b) extraordinary wave.

frequency ($Z \ll 1$), the imaginary part of the effective permittivity is proportional to the product of the collision frequency by the square of the electron density: $\varepsilon_i \sim \nu Z \sim N^2\nu_e$. As the altitude decreases below the E layer, the electron density decreases and the collisions frequency increases (see Figs. 1 and 2); therefore, the maximum absorption takes place near the lower boundary of the ionosphere, as can be seen in Figs. 6 and 7. Figure 6 shows the dependences on the absorption Ψ on the altitude along the trajectories (in Np).

In Fig. 6, two groups of curves can be distinguished. For rays at higher frequencies, passing through the ionosphere, the absorption is small. Rays at lower frequencies are reflected from the layer. The characteristic maximum on the curves is the reflection point. These rays spend much time in the lower ionosphere and undergo active absorption. Naturally, with decreasing frequency, the absorption increases and, comparing Figs. 6a and 6b, we see that the extraordinary wave is absorbed more intensely than the ordinary wave.

Figure 7 shows local absorption along ray paths. The graphs in Fig. 7 were plotted by formula (19). In Fig. 7, we clearly see an increase in absorption with decreasing frequency; moreover, the absorption is affected by a small region along the lower boundary of the ionosphere. Since, in the generally accepted models, the data on the collision frequency and electron density below 65 km are usually not presented, it is clear that this region has been studied insufficiently. We do not present the graphs of the imaginary part of

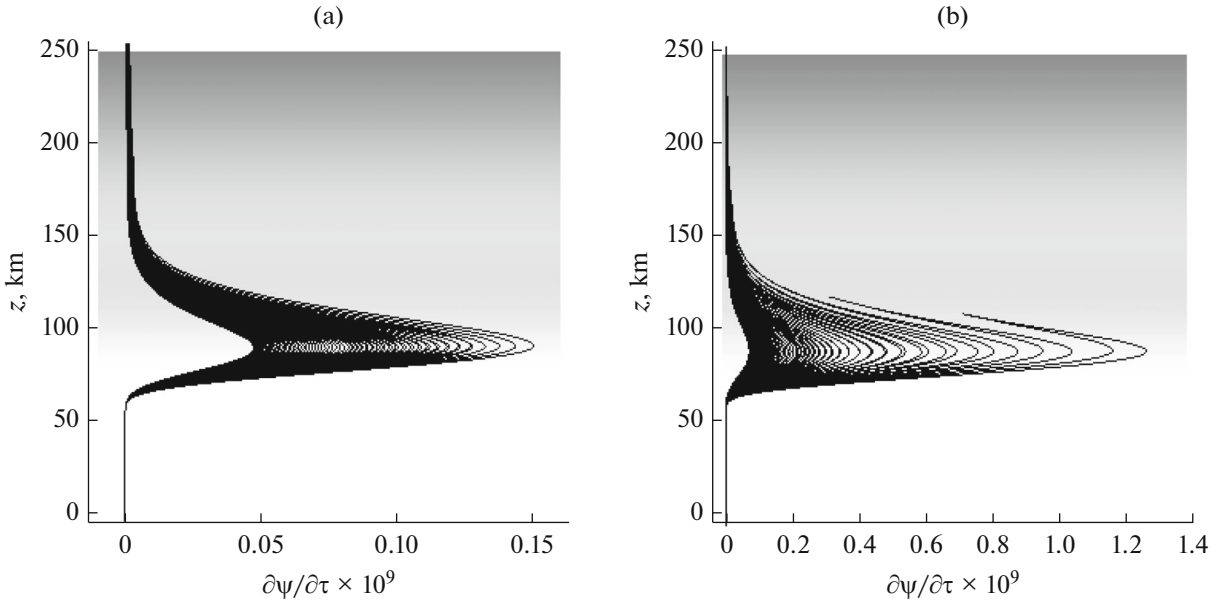

Fig. 7. Local absorption along ray paths vs. altitude: (a) ordinary wave and (b) extraordinary wave.

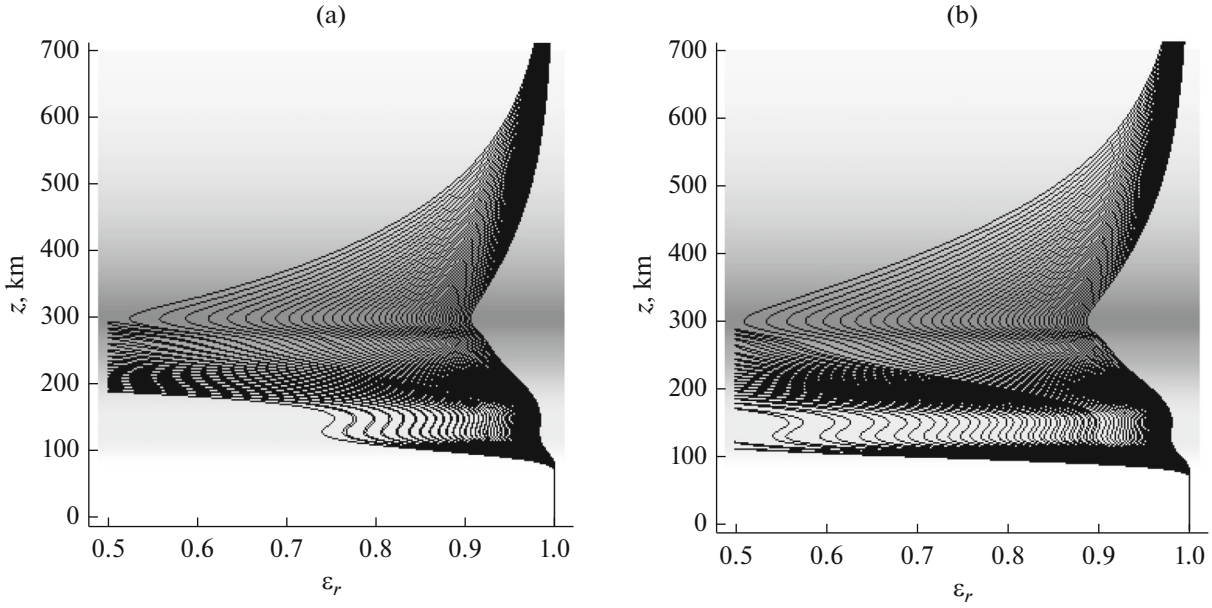

Fig. 8. Real part of the effective permittivity of the medium along the ray paths vs. altitude: (a) ordinary wave and (b) extraordinary wave.

the effective permittivity, since, by virtue of (19), they are similar to Fig. 7.

Figure 8 shows the dependences on the altitude for the real part of the effective permittivity of the medium along the ray paths. The right part of the figures is bounded by 1 (permittivity in a vacuum), and the left part, by 0.5, which is determined by the ray departure angle α_0. Since the effective permittivity depends on the coordinates, as well as on the wave vector and the frequency of the signal, each ray has an individual dependence on the altitude. The minima correspond to the *E* and *F* layers. The dependences for the ordinary (see Fig. 8a) and extraordinary waves (see Fig. 8b) are very similar. It should be noted that, as follows from the calculations, the allowance for the effective collision frequency has no significant effect on the ray path. This makes sense if we consider that the correction for ε_r is proportional to $\nu Z^2 \sim N^2\nu_e^2$.

Figure 9 shows the dependences of the divergence along the ray paths on the altitude (in decibels).

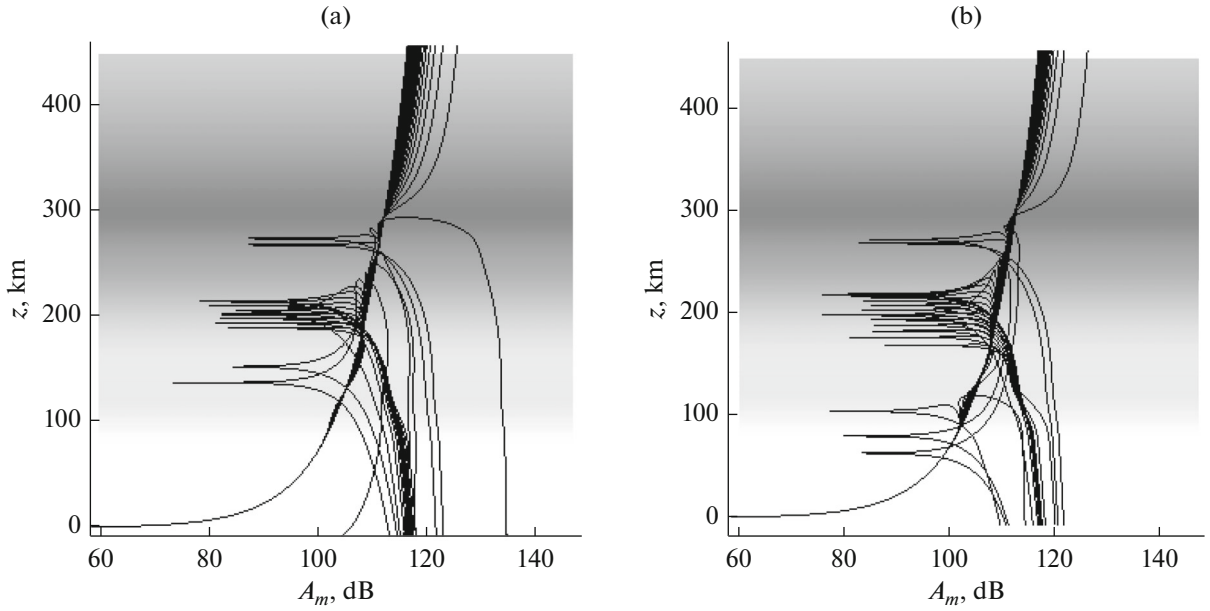

Fig. 9. Divergence along the ray paths vs. altitude (in decibels): (a) ordinary wave and (b) extraordinary wave.

To determine the divergence, it is necessary to transform bicharacteristic system (8) to

$$\frac{d\vec{k}}{dt} = \frac{\partial\omega^2\varepsilon}{\partial\vec{r}}\Big/\frac{\partial\omega^2\varepsilon}{\partial\omega}, \quad \frac{d\vec{r}}{dt} = \left(2c^2\vec{k} - \frac{\partial\omega^2\varepsilon}{\partial\vec{k}}\right)\Big/\frac{\partial\omega^2\varepsilon}{\partial\omega}, \quad (20)$$

known as Lukin's bicharacteristic system [21, 22], and complement it with the system of equations

$$\begin{aligned}
\frac{d\vec{k}_{\alpha_0}}{dt} &= \frac{\partial}{\partial\alpha_0}\left(\frac{\partial\omega^2\varepsilon}{\partial\vec{r}}\Big/\frac{\partial\omega^2\varepsilon}{\partial\omega}\right),\\
\frac{d\vec{r}_{\alpha_0}}{dt} &= \frac{\partial}{\partial\alpha_0}\left(\left(2c^2\vec{k} - \frac{\partial\omega^2\varepsilon}{\partial\vec{k}}\right)\Big/\frac{\partial\omega^2\varepsilon}{\partial\omega}\right),\\
\frac{d\vec{k}_{\beta_0}}{dt} &= \frac{\partial}{\partial\beta_0}\left(\frac{\partial\omega^2\varepsilon}{\partial\vec{r}}\Big/\frac{\partial\omega^2\varepsilon}{\partial\omega}\right),\\
\frac{d\vec{r}_{\beta_0}}{dt} &= \frac{\partial}{\partial\beta_0}\left(\left(2c^2\vec{k} - \frac{\partial\omega^2\varepsilon}{\partial\vec{k}}\right)\Big/\frac{\partial\omega^2\varepsilon}{\partial\omega}\right),
\end{aligned} \quad (21)$$

with the initial conditions

$$\begin{aligned}
k'_{x\alpha_0}(\eta) &= -\frac{\omega}{c}\sqrt{\varepsilon_0}\sin\alpha_0\cos\beta_0,\\
k'_{x\beta_0}(\eta) &= -\frac{\omega}{c}\sqrt{\varepsilon_0}\cos\alpha_0\sin\beta_0,\\
k'_{y\alpha_0}(\eta) &= -\frac{\omega}{c}\sqrt{\varepsilon_0}\sin\alpha_0\sin\beta_0,\\
k'_{y\beta_0}(\eta) &= \frac{\omega}{c}\sqrt{\varepsilon_0}\cos\alpha_0\cos\beta_0,\\
k'_{z\alpha_0}(\eta) &= \frac{\omega}{c}\sqrt{\varepsilon_0}\cos\alpha_0, \quad k'_{z\beta_0}(\eta) = 0,\\
\vec{r}'_{\zeta}(\eta) &= 0, \quad \vec{r}'_{\beta_0}(\eta) = 0,
\end{aligned} \quad (22)$$

i.e., to solve an extended bicharacteristic system [4, 21, 22].

Having obtained the solution of bicharacteristic system (21), we can calculate the Jacobian J of the divergence of a ray tube:

$$J = \begin{vmatrix} \frac{\partial x}{\partial\alpha_0} & \frac{\partial x}{\partial\beta_0} & T_1\\ \frac{\partial y}{\partial\alpha_0} & \frac{\partial y}{\partial\beta_0} & T_2\\ \frac{\partial z}{\partial\alpha_0} & \frac{\partial z}{\partial\beta_0} & T_3 \end{vmatrix}, \quad \vec{T} = \left(2c^2\vec{k} - \frac{\partial\omega^2\varepsilon}{\partial\vec{k}}\right)\Big/\frac{\partial\omega^2\varepsilon}{\partial\omega} \quad (23)$$

and find the divergence of the field at each point of space:

$$A_m = 10\log\left|\frac{J_0}{J(\vec{r})}\right|. \quad (24)$$

In formula (24), J_0 is the Jacobian of the divergence at a given distance from the source (in the calculations, it was taken equal to 1 m). We have $\varepsilon = \varepsilon_r$.

In Fig. 9, in the first turn, it is worth noting the trajectory corresponding to the high-frequency signal. It has a small kink in the vicinity of the maximum of the F layer, which is related to signal defocusing. The horizontal lines correspond to caustics. These are areas of field amplification (focusing). It follows from Fig. 9 that the rays corresponding to long-range propagation (see Fig. 3), sometimes called Pedersen rays, undergo a very large divergence.

Using the data presented in Figs. 3, 6, and 9, we can estimate the signal amplitude at the reception point.

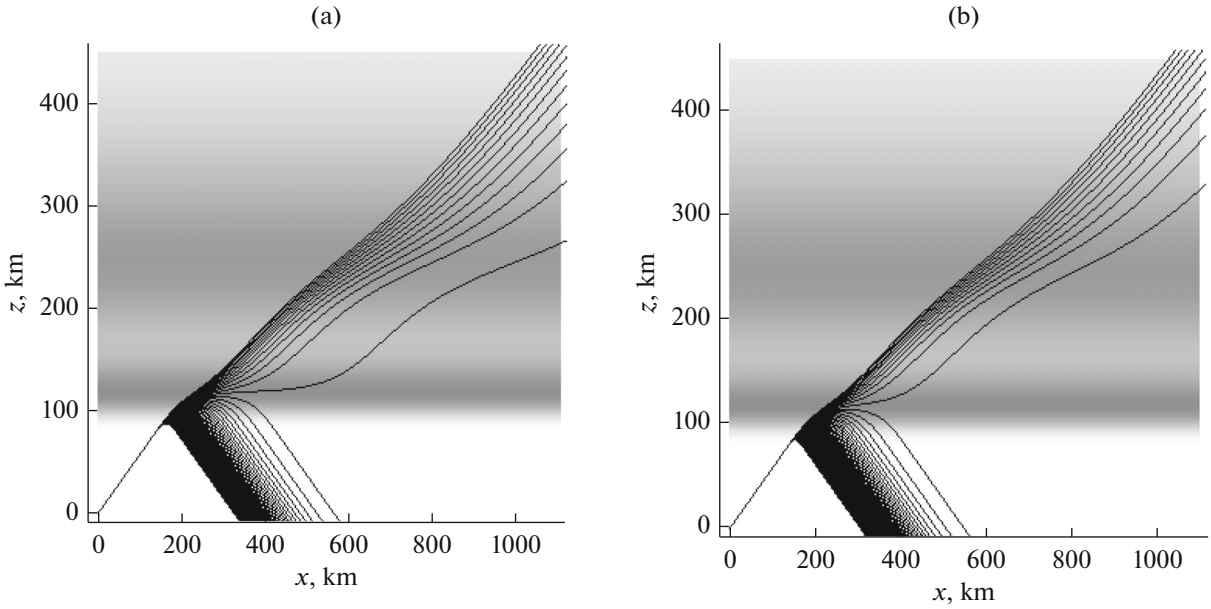

Fig. 10. Ray structure of a chirp signal in the plane (*x, z*): (a) ordinary wave and (b) extraordinary wave.

As is known, the effective electric field of an isotropic radiator in a vacuum is determined by the formula

$$E_{e0} = \frac{\sqrt{30W}}{r},\ \text{V/m}, \qquad (25)$$

where W [W] is the power and r [m] is the distance to the radiation source. Then, the effective electric field at an arbitrary point in space can be evaluated by the formula

$$E_e = E_{e0}\exp(-\psi)\times 10^{-A_m/20},\ \text{V/m}. \qquad (26)$$

For example, for the nighttime ionosphere, for a signal frequency of ~4 MHz on the ground (800 km from the source), the absorption is on the order of 1 Np and the divergence is about 120 dB. If we assume that the source power is 1 kW, then the field strength at this point will be 64 μV/m.

3. NUMERICAL SIMULATION. DAYTIME IONOSPHERE

Let us now consider the corresponding graphs for the daytime ionosphere (Figs. 10–16) for ordinary and extraordinary waves. The beam departure angle is 30°.

Figure 10 shows the beam structure of a chirp signal in the (*x, z*) plane. Since, in this case, the maximum of the *E* layer is greater than the maximum of the *F* layer, which is an anomaly, the rays are reflected only from the *E* layer (compare with Fig. 3). If we compare it with the ray structure of the nighttime ionosphere, then the communication range at the same frequency at a fixed beam departure angle has noticeably decreased (more than by a half) and the structure has become more ordered.

Figure 11 shows the ray structure of a chirp signal in the lateral plane (*y, z*). The main difference from the night ionosphere (see Fig. 4) is that the rays deviate less from the original plane of propagation.

Figure 12 shows the top view of the ray structure, i.e., the ray structure of a chirp signal in the (*x, y*) plane. If we compare the trajectories in this plane for the daytime (see Fig. 12) and the nighttime ionosphere (see Fig. 5), then we see again that the reflected rays deviate less from the original plane of propagation, which is consistent with Fig. 11.

Figure 13 shows the dependence on the altitude of the absorption Ψ along the trajectories. Comparing the absorption in the daytime (see Fig. 13) and the nighttime ionosphere (see Fig. 6), we see that it has increased significantly. The maximum absorption for an ordinary wave is approximately 8.5 Np, and, for an extraordinary wave, ~22.5 Np. For a frequency of ~4 MHz, the absorption is ~7 Np for an ordinary wave and ~ 10 Np for an extraordinary wave.

Figure 14 shows the local absorption along the ray paths. If we compare the nighttime (see Fig. 7) and daytime ionosphere (see Fig. 14), we see that the peaks have become narrower and much longer. They are still located near the lower boundary of the ionosphere.

Figure 15 shows the dependences on the altitude of the real part of the effective permittivity of the medium along the ray paths. In comparison with Fig. 8, the character of curves in Fig. 15 has changed significantly. They became more compact, since the behavior of the curves follows the behavior of the electron density (compare Figs. 1a and 1b).

Figure 16 shows the dependence on the altitude of the divergence along the ray paths (in decibels). As in

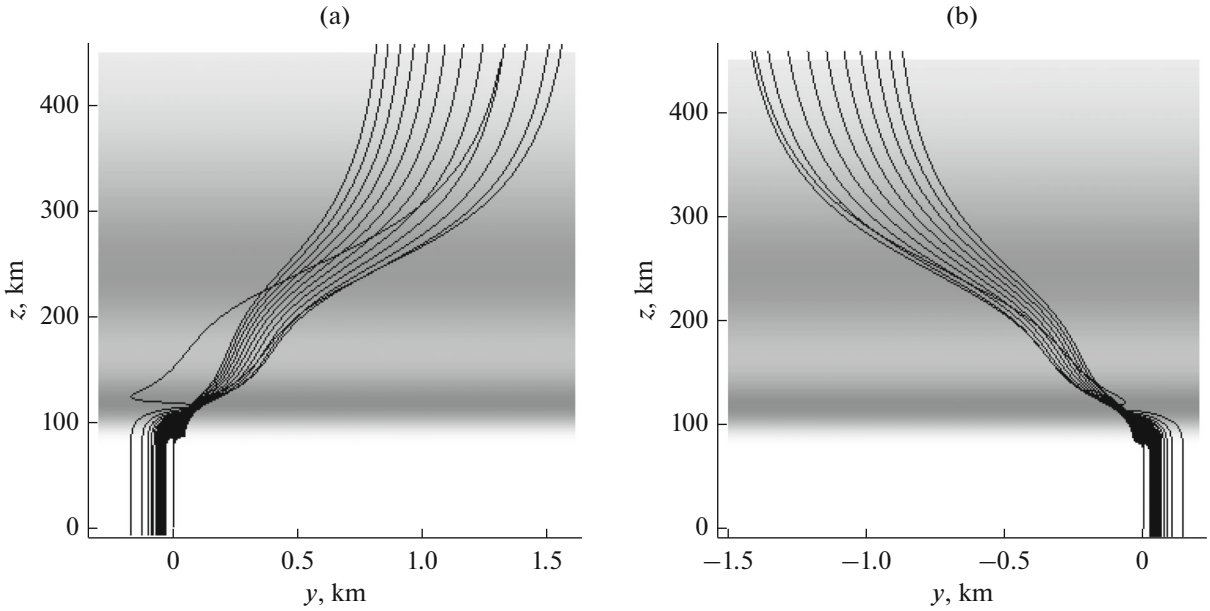

Fig. 11. Ray structures of a chirp signal in the plane (*y, z*): (a) ordinary wave and (b) extraordinary wave.

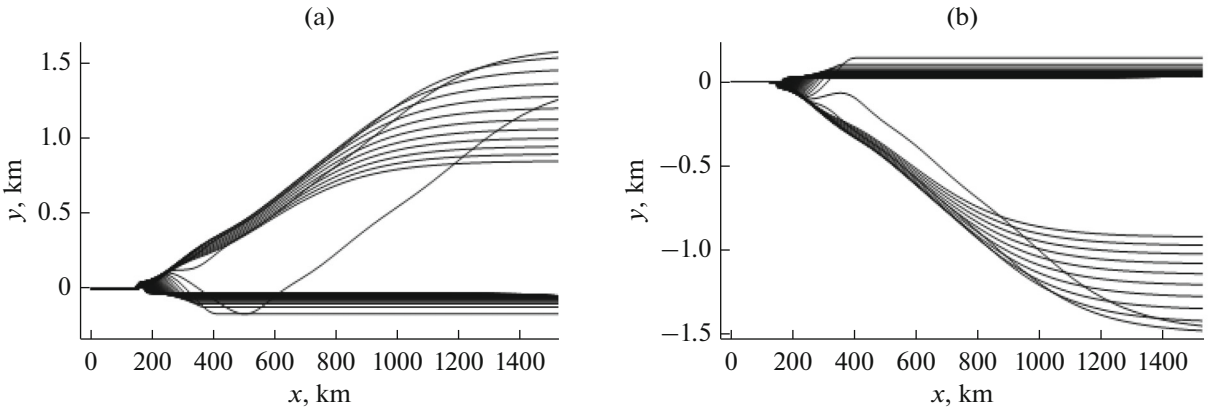

Fig. 12. Ray structures of a chirp signal in the plane (*x*, *y*): (a) ordinary wave and (b) extraordinary wave.

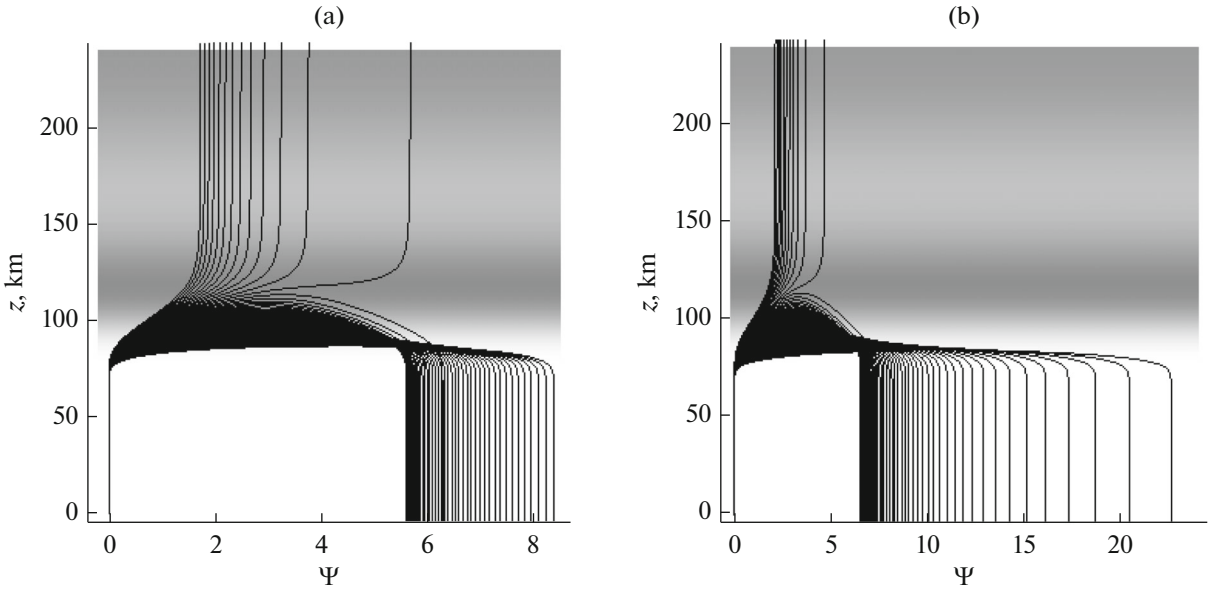

Fig. 13. Absorption Ψ (in Nepers) along trajectories vs. altitude: (a) ordinary wave and (b) extraordinary wave.

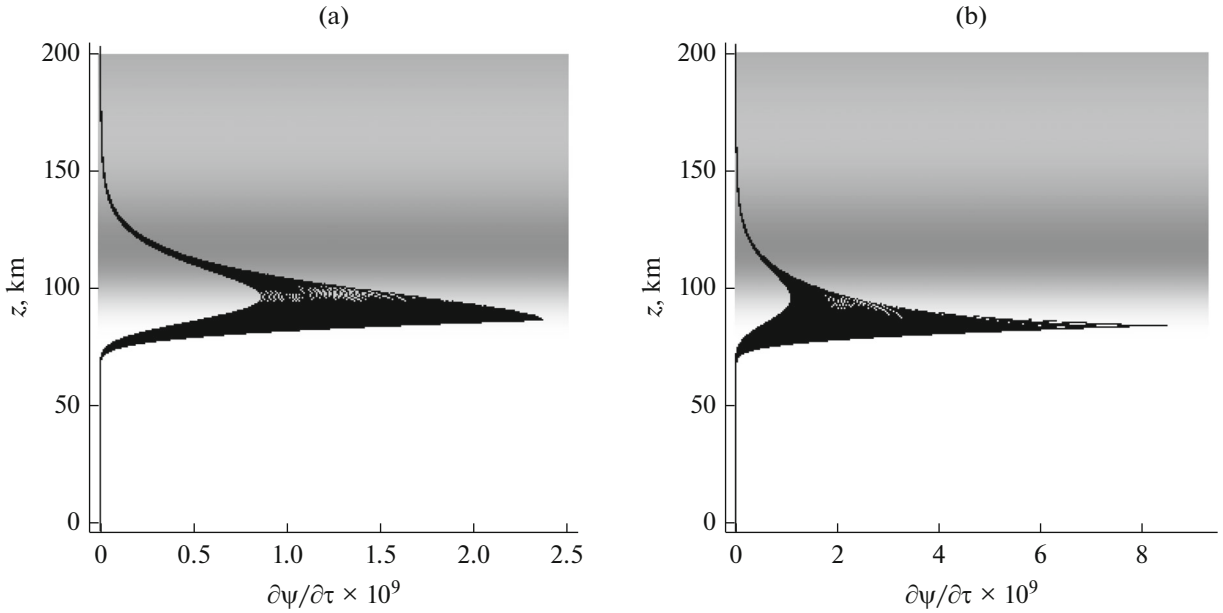

Fig. 14. Local absorption along ray paths vs. altitude: (a) ordinary wave and (b) extraordinary wave.

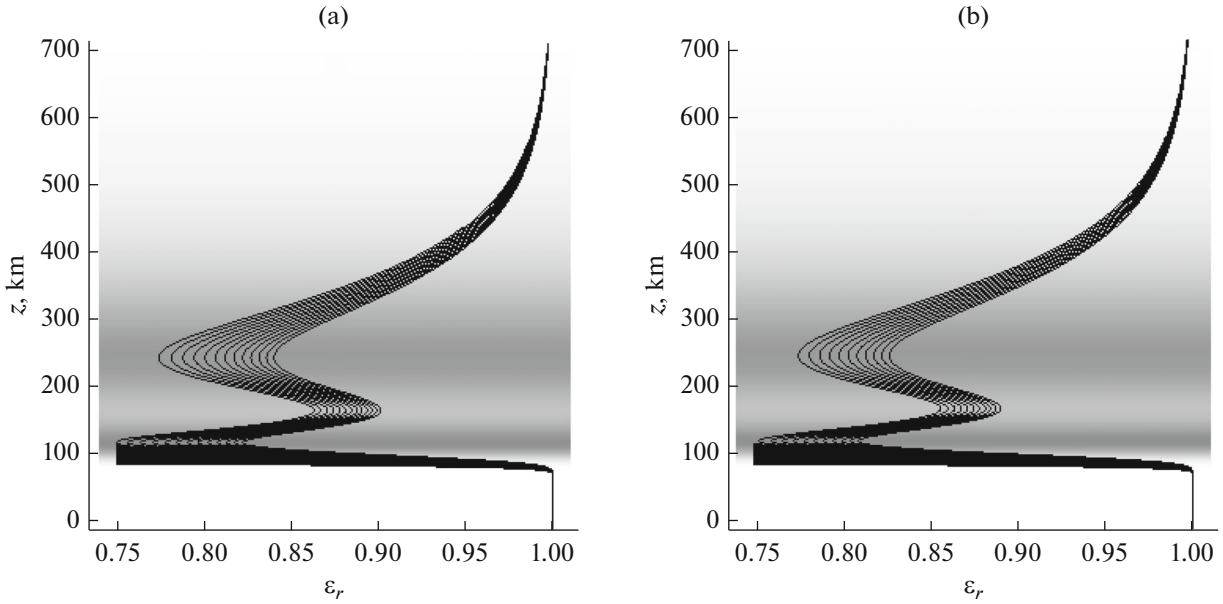

Fig. 15. Real part of the effective permittivity of the medium along the ray paths vs. altitude: (a) ordinary wave and (b) extraordinary wave.

the case of the nighttime ionosphere, using Figs. 10, 13, and 16, one can estimate the signal amplitude at the reception point. For rays with a frequency of ~4 MHz on the ground (distance of ~350 km from the source), the absorption is about 7 Np for an ordinary wave and 10 Np for an extraordinary wave and the divergence is about 115 or 110 dB, respectively. If we assume that the source power is 1 kW, then the field strength at this point will be 0.28 μV/m for an ordinary wave and 0.025 μV/m for an extraordinary wave.

CONCLUSIONS

Thus, in this paper, we have mathematically simulated the propagation of radio waves in the ionosphere with allowance for the Earth's magnetic field, frequency modulation, and the effect of the electron collision frequency on the deflecting absorption. The features of the propagation of chirp signals in a two-layer anisotropic ionosphere in the case of ordinary and extraordinary waves have been compared. The absorp-

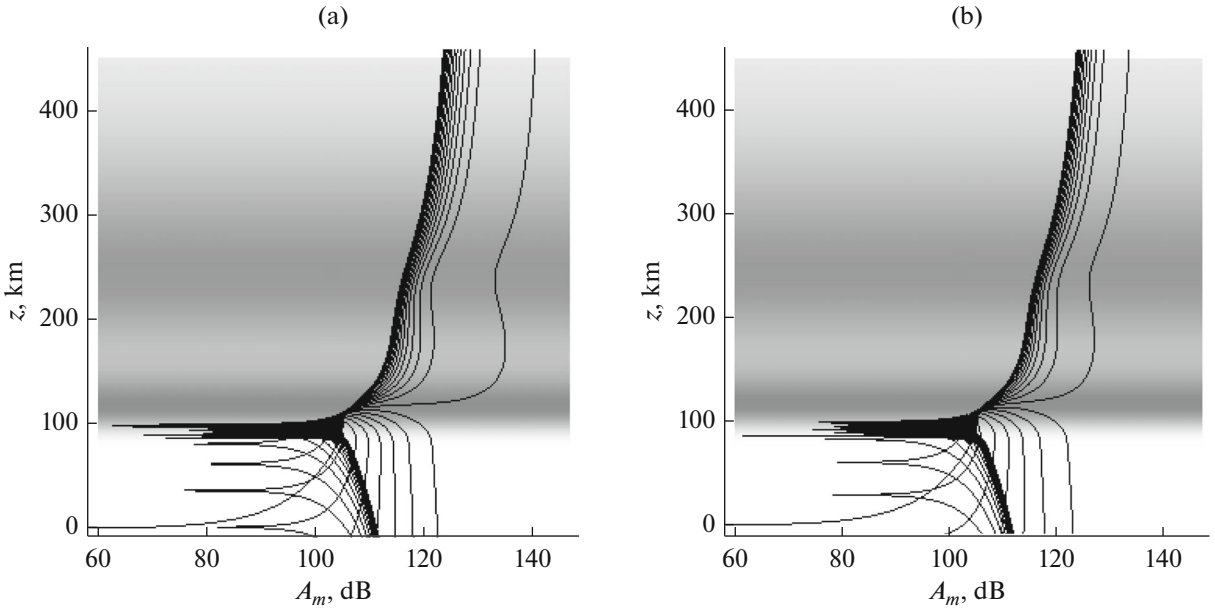

Fig. 16. Divergence along the ray paths vs. altitude (in decibels): (a) ordinary wave and (b) extraordinary wave.

tion of radio waves and the divergence along the rays and the influence of these factors on the attenuation of the radio signal have been studied. The calculations have been performed for daytime and nighttime models of the electron density of high-latitude ionospheric plasma. The projections of rays on different coordinate planes: the plane of propagation, the side plane, and the "top view", have been considered. The ray characteristics have been calculated using the bicharacteristic system of differential equations, the unknowns of which are the coordinates of the ray, the components of the wave vector, as well as frequency and time. The attenuation of the electric field along the trajectory was determined via calculating the divergence of the ray flux on the basis of an extended bicharacteristic system of equations.

The simulation results imply that, when studying the propagation of chirp signals in anisotropic media, it is necessary to calculate electromagnetic fields with a complex caustic structure using the wave catastrophe theory [15, 23–25], since, in order to describe the wave fields in accordance with the figures given above, it is necessary to calculate the fields on caustics (envelopes of ray families), including caustic singularities (catastrophes).

ACKNOWLEDGMENTS

This work was supported by the Russian Foundation for Basic Research, project nos. 18-02-00544-a and 17-02-01183-a.

REFERENCES

1. D. V. Ivanov, *Methods and Mathematical Models of the Research of Propagation in the Ionosphere of Complex Decameter Signals and Correction of Their Dispersion Distortions* (Mariiskii Gos. Tekh. Univ., Ioshkar-Ola, 2006).
2. V. A. Ivanov, D. V. Ivanov, A. R. Lashchevskii, and M. I. Ryabova, Vestn. Povolzh. Gos. Tekhnol. Univ., Ser. Radiotekh. Infokommut. Sist., No. 1(20), 43 (2014).
3. V. E. Zakharov and D. S. Kotova, in *Radio Wave Propagation (Proc. 24th All-Russian Sci. Conf., Irkutsk, June 29–July 5, 2014)* (ISZF SO RAN, Irkutsk, 2014), Vol. 4, p. 97 [in Russian].
4. A. S. Kryukovskii, D. S. Lukin, and K. S. Kir'yanova, J. Commun. Technol. Electron. **57**, 1039 (2012).
5. A. S. Kryukovskii, D. S. Lukin, and D. V. Rastyagaev, Elektromagn. Volny Elektron. Sist. **12** (8), 15 (2007).
6. A. S. Kryukovskii and I. V. Zaichikov, Elektromagn. Volny Elektron. Sist. **13** (8), 36 (2008).
7. K. S. Kir'yanova and A. S. Kryukovskii, T-Comm: Telekomm. & Transport, No. 11, 25 (2012).
8. A. S. Kryukovskii, D. V. Rastyagaev, and Yu. I. Skvortsova, Vestn. Ross. Novogo Univ., Ser. Upravl., Vychisl. Tekh. & Inf., No. 4, 47 (2013).
9. A. S. Kryukovskii, D. S. Lukin, D. V. Rastyagaev, and Yu. I. Skvortsova, J. Commun. Technol. Electron. **60**, 1049 (2015).
10. A. S. Kryukovskii, D. S. Lukin, D. V. Rastyagaev, and Yu. I. Skvortsova, T-Comm: Telekomm. & Transport, **9** (9), 40 (2015).
11. A. S. Kryukovskii and Yu. I. Skvortsova, Vestn. Ross. Novogo Univ., Ser. Slozhnye Syst.: Modely, Analiz i Upravl., No. 1-2, 34 (2016).

12. Yu. I. Bova, Vestn. Rossiiskogo Novogo Universiteta, Ser. Slozhnye Syst.: Modely, Analiz & Upravl., No. 3, 10 (2016).

13. A. S. Kryukovskii and Yu. I. Skvortsova, Izv. Vyssh. Uchebn. Zaved., Fiz. **59** (12-3), 131 (2016).

14. K. Davies, *Ionospheric Radio Waves*, (Blaisdell, London, 1969).

15. D. S. Lukin and E. A. Palkin, *Numerical Canonical Method in Problems of Diffraction and Propagation of Electromagnetic Waves in Heterogeneous Environments* (MFTI, Moscow, 1982) [in Russian].

16. *GOST 25645.146-89 Earth's Ionosphere. Model of Global Distribution of Electron Density, Temperature, and Effective Collision Frequency* (Izd-vo Standartov, Moscow, 1990), Part 1 [in Russian].

17. A. S. Kryukovskii and D. S. Lukin, Radiotekh. Elektron. (Moscow) **26**, 1121 (1981).

18. A. S. Kryukovskii, D. S. Lukin, and E. A. Palkin, Izv. Vyssh. Uchebn. Zaved., Radiofiz. **29**, 79 (1986).

19. A. S. Kryukovskii and D. V. Rastyagaev, in *Propagation and Diffraction of Waves in Heterogeneous Media* (MFTI, Moscow, 1989), p. 56 [in Russian].

20. A. S. Kryukovskii and D. V. Rastyagaev, in *Diffraction and Propagation of Electromagnetic Waves* (MFTI, Moscow, 1993), p. 20 [in Russian].

21. A. N. Kazantsev, D. S. Lukin, and Yu. G. Spiridonov, Kosm. Issl. **5**, 593 (1967).

22. D. S. Lukin and Yu. G. Spiridonov, Radiotekh. Elektron. (Moscow) **14**, 1673 (1969).

23. A. S. Kryukovskii, *Uniform Asymptotic Theory of Edge and Angular Wave Catastrophes* (RosNOU, Moscow, 2013) [in Russian].

24. A. S. Kryukovskii and Yu. I. Skvortsova, Elektromagn. Volny Elektron. Sist. **18** (8), 18 (2013).

25. T. V. Dorokhina, A. S. Kryukovskii, and D. S. Lukin, Elektromagn. Volny Elektron. Sist. **12** (8), 71 (2007).

Translated by E. Chernokozhin